Title

Linking Perfluorosulfonic Acid Ionomer Chemistry and High-Current Density Performance in Fuel-Cell Electrodes

Journal

ACS Applied Materials & Interfaces, 13(36)

ISSN

1944-8244

Authors

Chowdhury, Anamika

Bird, Ashley

Liu, Jiangjin

et al.

Publication Date

2021-09-15

DOI

10.1021/acsami.1c07611

Peer reviewed

Linking PFSA Ionomer Chemistry and High Current-Density Performance in Fuel-Cell Electrodes

*Anamika Chowdhury[1,2], Ashley Bird[1,2], Jiangjin Liu[2], Iryna V. Zenyuk[3], Ahmet Kusoglu[2], Clayton J. Radke[1], and Adam Z. Weber[2]**

[1]Energy Conversion Group, Energy Technologies Area, Lawrence Berkeley National Laboratory, Berkeley, California 94720, USA

[2]Department of Chemical and Biomolecular Engineering, University of California, Berkeley, California 94720, USA

[3]Department of Chemical and Biomolecular Engineering, University of California, Berkeley, California 94720, USA

*Corresponding author, Email: azweber@lbl.gov

Keywords: PEFC electrodes, mass transport, ionomer content, ionomer chemistry, equivalent weight, limiting current

ABSTRACT

Transport phenomena are key in controlling performance of electrochemical energy-conversion technologies and can be highly complex involving multiple length-scales and materials/phases. Material designs optimized for one reactant species transport however may inhibit other transport processes. We explore such trade-offs in the context of polymer-electrolyte fuel-cell (PEFC) electrodes, where ionomer thin films provide the necessary proton conductivity but retard oxygen transport to the Pt reaction site and cause interfacial resistance due to sulfonate/Pt interactions. We examine electrode overall gas-transport resistance and its components as a function of ionomer content and chemistry. Low equivalent-weight ionomers allow better dissolved-gas and proton transport due to greater water uptake and low crystallinity, but also cause significant interfacial resistance due to high density of sulfonic-acid groups. These effects of equivalent weight are also observed via *in-situ* ionic conductivity and CO displacement measurements. Of critical importance, the results are supported by *ex-situ* ellipsometry and x-ray scattering of model thin-film systems, thereby providing direct linkages and applicability of model studies to probe complex heterogeneous structures. Structural and resultant performance changes in the electrode are shown to occur above a threshold sulfonic-group loading highlighting the significance of ink-based interactions. Our findings and methodologies are applicable to a variety of solid-state energy-conversion devices and material designs.

INTRODUCTION

Multicomponent porous electrodes find applications in a wide variety of electrochemical energy conversion devices such as polymer-electrolyte fuel cells (PEFCs), CO_2 reduction, batteries, *etc*.[1-3] These structures allow transport of different reactant species in different phases while maintaining high interfacial surface area where electrochemical reactions occur. Efficient transport processes allow for high catalyst utilization and optimal device performance but are difficult to interrogate because of the complex electrode structure rendered by multiple intercalating phases. In PEFCs, the porous electrode consists of carbon agglomerates dispersed with Pt nanoparticles, bound together by an ion-conducting polymer (ionomer). Prior imaging studies, utilizing a wide range of techniques, highlight the heterogeneity in CL structure due to non-uniform ionomer distribution, wide distribution in agglomerate sizes and shapes, *etc*. [4-8] Such non-uniformities impact local transport properties, subsequently affecting species transport and power output. [9-11]

Gas-transport loses currently limit the high-current-density performance of PEFC electrodes.[12-13] Several studies established the presence of a high local gas-transport resistance near the Pt sites, which is attributed to the ionomer thin film and its associated Pt/ionomer interactions.[7, 12, 14-16] Additionally, the local gas-transport resistance increases as Pt loading is reduced with the local resistance scaling with the inverse of Pt-specific surface area.[7, 15, 17] This presents a significant challenge since the use of high Pt content in these systems makes them prohibitively expensive for wide-scale commercialization.[12-13]

Several *ex-situ* and model studies have emerged to study the properties of ionomer thin films. Their applicability to heterogeneous multiphase PEFC electrodes, however, has not been

sufficiently rationalized. By utilizing techniques such as quartz-crystal microbalance (QCM)[18-20] and ellipsometry[19-22] for mass- and thickness-change measurements, respectively; grazing-incidence small-angle and wide-angle X-ray scattering;[20-24] neutron reflectivity;[18] and transmission-electron microscopy,[21] the morphology of thin films cast on planar substrates is found to be significantly different from that of bulk ionomer. Confinement effects that emerge as film thickness approaches a characteristic domain size of the polymers and substrate/surface specific interactions can influence the orientation of ionomer backbone chains causing anisotropic chain alignment and altered transport properties, such as lower water and oxygen diffusivities, ionic conductivity, water uptake, overall swelling, and swelling rates.[18-21, 25-28]

The ionomer/Pt interface has also received scrutiny due to possible sulfonic-group/Pt interactions resulting in catalyst poisoning at certain applied potentials and/or formation of a dense ionomer layer near the Pt surface. Rotating-disk-electrode studies report an increase in electrode activity when using alternate electrolytes such as perchloric acid instead of Nafion.[29-30] Kodama *et al.*[31] used a novel ionomer with a sulfonamide anionic side-group and observed better performance compared to Nafion, potentially due to weaker adsorption strength of sulfonamide group, resulting in lower catalyst poisoning. Modeling and simulation studies involving density-functional theory (DFT) and molecular dynamics (MD) also suggest the presence of an additional interfacial resistance at Pt/ionomer interface due to anionic side-group/Pt interaction, resulting in formation of a dense ionomer layer with reduced reactant-gas permeability close to the Pt surface.[31-33] Recently, Garrick *et al*.[34] quantified anion adsorption on Pt in PEFC electrodes via CO adsorption measurements, reporting an increase in anion adsorption (also referred to as catalyst poisoning) with increasing ionomer content. Overall, these available studies reveal a

wide range of probable sources for the local-gas transport resistance, which may occur simultaneously and synergistically.

In our previous studies, we used *in-situ* characterizing techniques to conclude that electrode gas-transport resistance consists of transport resistance through electrode secondary pores and a local gas-transport resistance close to Pt particles due to the ionomer thin film.[35-36] This local gas-transport resistance is further sub-divided into two components: (i) diffusional transport resistance through ionomer thin film, and (ii) an interfacial resistance either at the gas/ionomer or at the ionomer/Pt interface.[35-36] The individual components of local gas-transport resistance were quantified using pressure and molecular-weight dependence of the component resistances. Despite accounting for an interfacial resistance, the thin-film permeability was found to be an order of magnitude lower than bulk-ionomer permeability, thus confirming that the properties of ionomer thin film are different from those of the bulk ionomer. The relative contribution of component resistances depends on several parameters, including ionomer to carbon weight ratio (I:C ratio), proximity of Pt particles to ionomer thin film, and Pt to carbon weight ratio (Pt:C wt. %).[36-37]

As discussed above, several *in-situ* studies of transport resistance in PEFC electrodes and *ex-situ* studies of ionomer suggest that the ionomer thin film is the source of local resistance. Consequently, optimizing ionomer chemistry to improve ionomer thin-film transport properties becomes important. Recent research has focused on developing and characterizing ionomers with lower equivalent weight (EW) – the inverse of ion-exchange capacity – and shorter side-chain chemistries.[38-40] Most studies to date characterizing new ionomer chemistries have utilized *ex-situ* model studies, which have not been directly linked to *in-situ* experiments. In a recent study by

Ramaswamy *et al.*,[41] ionomer EW was identified as the dominant property (over side-chain length) on local gas-transport resistance and bulk H^+ transport resistance. Electrodes with low EW ionomers demonstrated better ion and gas transport, potentially due to higher water uptake. However, the electrodes with varying ionomer EW and/or side-chain length were fabricated from inks with constant sulfonic-acid molality, as opposed to I:C mass ratio typically used in PEFC electrodes. Consequently, electrodes with low EW had low I:C ratio. Our previous study demonstrates that electrodes with low I:C ratio exhibit low gas-transport resistance.[35] Thus, it is unclear whether the improvement in gas-transport in electrodes with low EW is due to low ionomer content or to an intrinsic ionomer property (*e.g.*, water uptake). Moreover, the presented trends do not provide insight into the impact on interfacial resistance, which potentially results from sulfonic-group/Pt interactions and hence, sulfonic-group density. In electrodes with low EW ionomer, interfacial resistance may dominate over the transport resistance through the ionomer thin film, thus resulting in high gas-transport resistance, which was observed in the study of Ono *et al.* with low-EW ionomer and constant I:C ratio (across all electrodes).

In this paper, we aim to address these questions by examining the trends in overall and component electrode transport resistance with different ionomer chemistries (EW and side-chain chemistry), and ionomer content, using a combination of *in-* and *ex-situ* techniques. We study ionomers: 3M 825 EW, 3M 1000 EW ionomers and Nafion (1100 EW). 3M 825 EW and 3M 1000 EW have the same side-chain but different side-chain density. Nafion, with an EW of 1100, has the same side-chain density as 3M 1000 EW, but a longer and more hydrophilic side-chain due to the presence of an additional ether-oxygen group. For brevity, we refer to these differences in side-chain density, length, and oxygen-content as differences in ionomer

chemistry. Our results provide guidance in how to ameliorate the local resistance with the effects traced back to their initial causalities. The structure of the paper is as follows. First, we explore the dependence of overall and component electrode transport resistances on I:C ratio and ionomer chemistry utilizing a H_2-pump configuration as described by Schuler *et al*.[35] *In-situ* ion adsorption on a Pt surface and ionic conductivity measurements are employed to infer ionomer/Pt interaction and water uptake, and subsequent impact on transport properties. Next, the observed trends are compared with model-system *ex-situ* water uptake measurements and with x-ray scattering data reproduced from Kusoglu *et al*.[22] Lastly, we demonstrate the impact of I:C ratio on ink properties, electrode structure, and subsequently, on limiting-current performance.

EXPERIMENTAL METHODS

Results presented in subsequent sections utilize several experimental methods from prior studies that are summarized below; the reader is referred to the SI for additional details on experimental methods.

Samples

Inks: All catalyst inks were prepared using earlier established protocol.[42] Ionomer dispersions (3M 825 EW, 3M 1000 EW, and Nafion® D521) and Pt-Vulcan catalyst particles (TEC10V10E, TEC10V30E and TEC10V50E from TKK, Tokyo, Japan) were dispersed in 1:1 n-propyl alcohol and deionized water mixture (by wt.). This was followed by manual agitation and bath sonication to disperse the mixture uniformly. Ink zeta potential was determined via electrophoretic light scattering technique (NanoPlus3, Micromeritics, Georgia, USA).

Electrode fabrication: The working electrode (WE) catalyst layers with varying ionomer chemistries and I:C ratios were spray-coated onto Nafion NR 212 membrane (Ion Power, Delaware, USA), while the counter electrodes (CEs) were spray-coated on the gas-diffusion layer (GDL) (Sigracet 25BC, SGL Wiesbaden, Germany) using a Sono-Tek ultrasonic spray coater (Sono-Tek Exacta Coat, New York, USA). The WE and CE Pt-loadings were held constant at 0.05 and 0.3 mg/cm^2, respectively, and a constant I:C ratio of 0.9 was maintained on the CEs.

In-Situ Test Protocol

Cell Assembly: Membrane-electrode-assemblies (MEAs), consisting of the spray-coated WE and CE stacked together (CE facing the Nafion membrane), were tested in a cell with single serpentine flow fields (Fuel Cell Technologies Inc, New Mexico, USA). The active area was limited to 2 cm^2 by covering remaining flow-channel area with Teflon gaskets. Commercial test stand (850e Multi-Range Fuel Cell Test System, Scribner Associates, North Carolina, USA) was used to control gas flowrates and cell operating conditions (cell temperature, RH, and pressure). Electrochemical measurements were recorded using a Biologic VSP potentiostat (Biologic, Seyssinet-Pariset, France).

Break-in protocol: A modified version of the break-in protocol described by Ono *et al.*[17] was adopted for this study. The samples were maintained at a constant potential (0.2 V referenced to the CE) for 12 hours at 80 °C, 100 % relative humidity (RH), and 50 kPa gauge pressure while flowing pure H_2 (flowrate of 400 std cm^3/minute) on CE side and air (flowrate of 800 std cm^3/minute) on WE side.

ECSA measurement: CO-stripping voltammetry, as described by Schuler *et al.*,[35] was utilized to measure electrochemically active surface area (ECSA). After CO adsorption, the WE potential

was scanned between 0.08 to 0.95 V, resulting in a transient current due to CO oxidation. CO-stripping charge, obtained by integrating the transient CO-peak, was used to calculate ECSA. A CO-monolayer oxidation charge of 420 mC/cm^2 was assumed in all the calculations. Operating conditions were same as those in transport-resistance measurements detailed below (via limiting-current experiments)

The surface-area roughness factor r_f, commonly used to characterize electrodes and defined as the ECSA normalized to electrode geometric area, was estimated from the ratio of ECSA to WE active area (2 cm^2 in our experiments).

Transport-resistance measurement: Electrode transport resistances were estimated from limiting-current measurements using the H_2-pump configuration and test protocol as described by Spingler *et al.*[43] and Schuler *et al.*[35] The cell was maintained at 40 °C, 80% RH and ambient pressure (0 kPa gauge backpressure). Total current density and crossover current density are recorded by flowing 1000 ppm H_2 diluted in Ar, and pure Ar, respectively, on the WE while maintaining a constant WE potential of 0.3 V (references to CE). 2% H_2 in Ar feed is maintained at the CE. Limiting current density is obtained by subtracting the crossover current density from total current density.

The total cell resistance R_{Total} is given by the ratio of average feed reactant concentration C_{Feed}^{Avg} (average of inlet feed concentration and outlet concentration) to the measured limiting current $i_{\lim ¿ ¿}$ as per

$$R_{Total} = \frac{nF\,C_{Feed}^{Avg}}{i_{\lim ¿ ¿}} \qquad (1)$$

where $n(¿2)$ is the number of electrons in the overall reaction. WE transport resistance, R_{WE}, is determined by subtracting the total GDL resistance$N\,R_{GDL}$ from R_{Total}.

Ionomer adsorption from CO displacement measurement: To quantify ionomer adsorption on the Pt surface, the CO displacement technique as described by Garrick *et al*. was employed. [34] In summary, CO when introduced into a well-equilibrated electrode displaces already adsorbed ions and produces a transient current. The magnitude of the calculated displacement charge is proportional to the amount of adsorbed species, while the sign of the transient current (positive or negative current) indicates the charge of adsorbed ions. We attribute cation adsorption to $H^{+¿¿}$ and anion adsorption to $SO_3^{-¿¿}$ species due to their abundance in the electrodes. Normalized coverage, θ, is defined as the displacement charge divided by the total charge from CO-stripping. The measurements were performed at the same operating conditions as the limiting current measurements.

H_2 pump EIS protocol: Electrode ionic conductivity was measured using the H_2-pump AC technique developed by Sabarirajan *et al*.[44] The pseudo-electrodes, *i.e*., electrodes without any Pt loading, with different ionomer chemistries and a constant I:C ratio of 0.6 were sandwiched between two membranes. This assembly was placed between the cathode and anode electrodes. Gas-diffusion electrodes (GDEs) with a Pt loading of 0.3 mg/cm^2 and an I:C ratio of 0.8 were used as anode and cathode electrodes. Ionic conductivity was estimated from EIS measurements conducted while flowing ultra-high purity H_2 on both electrodes at various operating RH and cathode potentials (references to the anode). The temperature and pressure were set to 80 °C and 100 kPa backpressure absolute, respectively.

***Ex-situ* measurements and data analysis**

Thin-film swelling (water-uptake) measurement: Swelling (water-uptake) measurements were conducted on unannealed thin films with the different ionomer chemistries using the experimental procedure described by Tesfaye *et al*.[45] Thin films were prepared by spin casting the dispersions onto a UV/ozone treated hydrophilic Pt substrate. Initial film thickness for all samples was measured via spectroscopic ellipsometry (J. A. Woollam alpha-SE, Nebraska, USA) to be 15 to 25 nm. Samples were dried in a vacuum oven for 1 h at 30 °C, and measured immediately after for swelling. The swelling measurements were conducted by monitoring the transient film thickness as a function of RH at ambient temperature using a spectroscopic ellipsometer with an incidence angle of 70°.

Swelling was determined by calculating the change in thickness ($\Delta\hat{\delta}=\hat{\delta}-\hat{\delta}_o$) at each RH step relative to the initial thickness at 0 % RH ($\hat{\delta}_o$). To convert swelling data to water content, λ (moles of water per mole of sulfonate groups), one-dimensional swelling of the thin film was assumed.[20] Assuming that no significant excess free volume or macroscale voids exist and additive pure molar volumes are valid, λ can be estimated from[18, 20, 46]

$$\lambda=\frac{mol\,H_2O}{mol\,SO_3^-}=\frac{\Delta\hat{\delta}}{\hat{\delta}_o}\frac{\rho_{H_2O}/MW_{H_2O}}{\rho_{ionomer}/EW_{ionomer}} \quad (2)$$

where ρ is density (dry density in case of ionomer), and *MW* is molecular weight. A dry density of 2.1 g/cm^3 was used for all ionomers.[46-47]

GISAXS intensity distribution analysis: Using the data reported by Kusoglu *et al*.,[22] we study the intensity distribution (I) of GISAXS patterns as a function of azimuthal angle (χ). The 2D-scattering pattern is divided into 2°-sector cuts over a χ-range of 6° to 68° after correcting for the

geometry. The region below 6° is excluded due to the signal from the specular rod overshadowing the ionomer peak. Similarly, the region greater than 68° is excluded due to interference from the Yoneda peak of Si.[48] Background signal is fit to a power-law function and then subtracted from each sector cut to account for the variation in background as a function of χ. The background-subtracted ionomer peak is fit to a gaussian function, integrated, and plotted as a function of χ. The error of the integral is calculated based on a 95 % confidence interval of the gaussian fit.

RESULTS AND DISCUSSION

In-situ electrode measurements:

Transport-resistance measurements: **Figure 1** (a) plots working electrode (WE) gas-transport resistance R_{WE} as a function of I:C ratio for the various ionomer chemistries. A constant low Pt-loading of 0.05 mg/cm^2 used in all examined samples resulted in a relatively constant roughness factor r_f of 52.83 ± 3.25 cm$^2_{Pt}$/cm$^2_{WE}$. Pt particles access H^+ through both ionomer and adsorbed water pathways.[37, 49] Hence, we observe a relatively constant r_f despite varying I:C ratio, which is expected to impact ionomer coverage.[8, 41] Nevertheless, R_{WE} measurements were normalized to the average r_f (see SI). For all ionomers, R_{WE} increases linearly with I:C ratio (highlighted in yellow box), consistent with literature trends.[35] At high I:C ratios, however, there is deviation from this linear trend with the deviation starting at different I:C ratios for the three different ionomers, which is discussed further in latter section. The current analysis is limited to the region of linear increase in R_{WE} with I:C ratio.

At low Pt loadings, the local gas-transport resistance dominates over the through-plane transport resistance.[7, 14, 17, 35] Within the linear regime, R_{WE} increases with increasing ionomer content due

to thicker films, as established by prior electrode-microstructure studies (see SI),[9-10] thereby resulting in higher through-ionomer transport resistance.

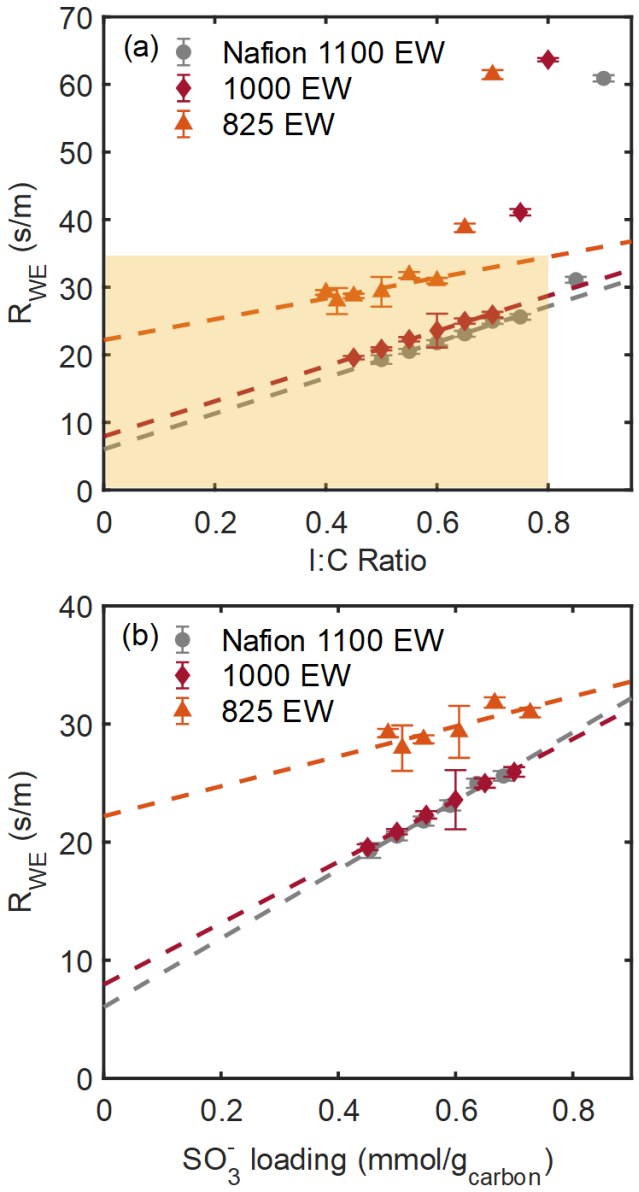

Figure 1: R_{WE} as a function of (a) I:C (weight) ratio, and (b) $SO_3^{-¿¿}$ group loading (mmol per gram carbon). Figure (b) plots only the linear region (highlighted in yellow box in Figure (a)). Measurements were done using the H_2 pump configuration for varying ionomer chemistries at 40 °C, 80 % RH, and ambient pressure (0 kPa gauge backpressure).

Although all three ionomer chemistries display a linear dependence of R_{WE} on I:C ratio, they have different intercepts and slopes (see SI for regressed values). The data are analyzed using a previously developed analytical model for R_{WE},[35]

$$R_{WE} = \frac{L}{3D_{WE}^{eff}} + \frac{R_{Local}}{\gamma r_f} \quad \frac{R_{Local}}{\gamma r_f} \tag{3}$$

where L is the thickness of electrode, D_{WE}^{eff} is the effective through-plane diffusivity of reactant gas, R_{Local} is the local gas-transport resistance close to Pt-site, r_f is the roughness factor, and γ is a correction factor included since only a fraction of Pt particles are active at limiting current. The first term, $L/3D_{WE}^{eff}$, is the through-plane resistance and is minimal at low Pt loadings (see SI for further verification).[7, 14, 17, 35] The second term, $R_{Local}/\gamma r_f$, is the total local gas-transport resistance summed over all active Pt particles and dominates at low Pt loadings. R_{Local} itself is composed of an interfacial resistance $R_{Pt/I}$, and a diffusive transport resistance through the ionomer thin film, δ/Π_{gas}.

$$R_{Local} = R_{Pt/I} + \frac{\delta}{\Pi_{gas}} \tag{4}$$

where δ is the effective ionomer thin-film thickness,[35] and Π_{gas} is the ionomer-thin-film dissolved-gas permeability. We attribute $R_{Pt/I}$ to the ionomer/Pt interface based on literature findings using both experimental and modeling techniques.[32-33] Increasing the I:C ratio increases δ,[9] while the interfacial component, $R_{Pt/I}$, determined by sulfonic group/Pt surface interactions, remains constant. Upon combining equations 3 and 4, R_{WE} is given by

$$R_{WE} = \frac{1}{\gamma r_f}\left(R_{Pt/I} + \frac{\delta}{\Pi_{gas}}\right), \textit{at low Pt loading}. \tag{5}$$

As mentioned above, total Pt loading, and thereby r_f, is constant across all examined samples. Additionally, we assume thatγ (which depend on agglomerate size and shape) remains constant since the carbon type and weight content, ink recipe, and fabrication process were identical across all samples. By comparing the above analytical model to experimental results and using I:C ratio as a proxy for δ, we observe that the intercept is proportional to $R_{Pt/I}$ and the slope is inversely proportional to Π_{gas}.

Comparison of 3M 825 EW and 1000 EW trends in Table S1 establish that a higher EW and therefore lower side-chain density results in a larger slope *i.e*, the ionomer thin-film transport resistance increases, whereas $R_{Pt/I}$, quantified from the intercept, decreases. The increase in ionomer thin-film transport resistance is justified based on water-uptake and crystallinity trends. The higher sulfonic-acid density for low EW samples promotes water uptake and reduces crystallinity, thus improving dissolved-gas permeability (known to increase with water uptake).[16] These conclusions are also supported by proton-conductivity measurements presented in SI, where pseudo-electrode with 825 EW ionomer consistently exhibits higher ionic conductivity compared to the 1000 EW pseudo-electrode across the entire examined RH range. Proton conductivity increases with higher ionomer water content and connectivity between hydrophilic anionic clusters in the electrode.[22] Since these two parameters are known to also enhance dissolved-gas permeability also, low EW ionomers likely possess higher dissolved-gas permeability.[21-22, 27] Simultaneously, the sulfonic-acid groups also interact with Pt surface resulting in formation of a dense layer close to the Pt surface and/or adsorb to the Pt surface under an applied potential thereby poisoning the catalyst. Both of these phenomena can cause large interfacial resistance.[31, 33-34]

As noted above, the results of 1000 EW and Nafion (1100 EW) ionomers highlight the impact of side-chain chemistry since the side-chain spacing (*i.e*., number of repeating tetrafluroethylene (TFE) units between side chains) is identical. From Figure 1, both 1000 EW and Nafion exhibit almost the same slope, *i.e*, they have similar transport properties. Nevertheless, the intercept capturing interfacial resistance increases for the 3M 1000 EW ionomer, suggesting that shorter side chains promote greater sulfonic-group/substrate interactions.

The above results indicate that local morphological behavior and substrate-specific interactions are governed by side-chain length, while side-chain density or spacing influences macroscopic properties such as water uptake and swelling and dominates the overall response. Similar observations have been made in previous *ex-situ* thin-film studies on a silicon substrate,[16, 22-24] thereby providing direct validation of these model studies to actual electrodes, as explored in more detail below. These observations are also in agreement with the conclusions by Ramaswamy *et al*. that state that the EW is the dominant ionomer property and low-EW ionomers aid in ion and reactant gas-transport due to higher water uptake.[41] They, however, attributed the trends to water uptake alone and did not observe any impact of interfacial resistance. This is probably due to the use of high-surface area carbon (HSC) support in their study. HSCs contain most of the Pt particles in interior micropores that inhibit ionomer infiltration due to size restrictions, and thus minimize interfacial resistance. In contrast, Figure 1 demonstrates a significant contribution of interfacial resistance due to the use of non-porous Vulcan carbon, where Pt particles are more likely to contact ionomer, and in agreement with Ono *et al.* who used Vulcan carbon.[17] This highlights the importance of considering the various

electrode microstructural parameters, such as distribution of Pt particles in carbon support, when optimizing for material properties (in this case ionomer EW).

An alternate method to analyze the above trends is to plot R_{WE} versus sulfonic-group loading or moles of sulfonic groups per gram carbon (*i.e.*, I:C ratio divided by EW), instead of I:C ratio, which is based on weight alone. This is shown in Figure 1(b) using the linear-region data points. The overall trend of a linear increase with a non-zero intercept is preserved. The intercepts remain the same as in Figure 1(a), reaffirming that the interfacial resistance is primarily a function of sulfonic-group density and local morphological properties at the substrate/ionomer interface (such as better chain alignment). The differences in slope are however exacerbated, while maintaining the same order *i.e*, 825 EW slope < 1000 EW slope < 1100 EW (Nafion) slope. The differences in slope increase because the length or mass of hydrophobic chain per mole of sulfonic group increases as EW increases. This increase translates to thicker films at the same sulfonic group loading (assuming the same ionomer thin-film density) for higher EW ionomers, thus leading to higher dissolved-gas transport-resistance. Note that the above conclusions assume γ and minimal contribution of through-plane transport resistance. The assumption of minimal contribution of through-plane transport resistance to the overall electrode gas-transport resistance agrees with several prior studies,[7, 14, 35] and is further verified in SI.

Anion adsorption from CO adsorption measurements: The above results qualitatively indicate preferential sulfonic-group/substrate interactions as a function of ionomer chemistry under limiting-current conditions (Pt utilization close to the external agglomerate surface). Ionic-species adsorption on the Pt-surface, indicative of ionomer/Pt interactions, can be directly quantified using CO-displacement technique.[34] Results in **Figure 2** plot normalized ion coverage

θ, estimated from the ratio of displacement charge during CO adsorption to the total charge from CO stripping, for the three different ionomers as a function of the constant WE potential applied during CO adsorption (referenced to the CE). At low applied potentials (0.15 V), positive displacement current is obtained indicating cationic species adsorption. At higher applied potentials (0.2 V and above), negative displacement current indicates anionic species adsorption. The potential of zero total charge (pzc), corresponding to no ion adsorption ($\theta=0$) *i.e.*, zero displacement current, lies between 0.17 to 0.19 V cell potential for all three ionomers when referenced to the CE (2 % H_2 balance Ar feed). Using a Nernstian correction, the pzc calculates to 0.27 to 0.29 V with reference to standard hydrogen electrode (1 atm H_2 feed at experimental temperature), which is in good agreement with literature reported pzc values for Pt.[34, 50-51] As the applied potential increases above the pzc, the Pt surface acquires greater positive charge, thereby resulting in increased anionic species adsorption. At a potential of 0.3 V, which is where our limiting-current measurements were recorded, the 825 EW ionomer electrode has the highest anion adsorption followed by the 1000 EW and then Nafion (1100 EW), again confirming that high sulfonic group density (between 3M 825 and 1000 EW), and short side-chain length enables greater ionomer/Pt interactions. Ionomer/Pt interactions can further result in catalyst poisoning and/or formation of a dense ionomer layer close to the Pt surface. Although the absence of a direct 1:1 correlation between $R_{Pt/I}$ measured from limiting-current experiments (Figure 1) and the normalized anion coverages (Figure 2) suggests that sulfonate/Pt interactions resulting in the formation of a dense layer close to Pt surface are primarily responsible for $R_{Pt/I}$, we cannot definitively make this conclusion because the CO-displacement technique utilizes all the Pt particles in the electrodes. The limiting-current experiment, on the contrary, is sensitive mainly to the Pt particles close to the agglomerate surface due to mass-transport limitations,[35] which are

more likely to contact ionomer.[9, 11] Consequently, the impact of sulfonate/Pt interactions is more prominent in limiting-current experiments relative to CO-adsorption measurements. Further studies are required to verify the exact phenomenon responsible for $R_{Pt/I}$.

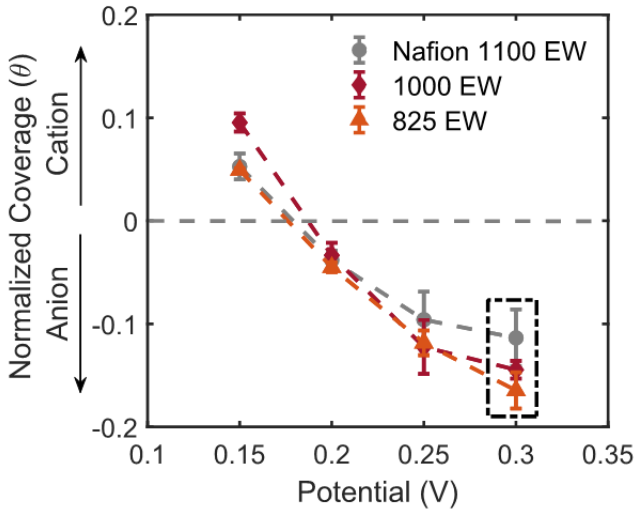

Figure 2: Normalized coverage (θ) of adsorbed ionic species on Pt surface versus applied constant potential for examined ionomers at 40 °C, 80 % RH, and ambient pressure (0 kPa gauge backpressure). All the examined WE samples maintained a constant Pt loading of 0.05 mg/cm^2 and I:C ratio 0.5. Coverage at 0.3 V (referenced to CE), where limiting-current measurements were performed, are highlighted in a box.

***Ex-situ* thin-film characterization:**

Water-uptake: To validate the above conclusions from *in-situ* experiments and compare with *ex-situ* studies, water uptake in terms of thin-film swelling (change in thin-film thickness relative to initial dry-state thickness) and λ were measured by ellipsometry for the different ionomer thin films on a Pt support with an oxidized surface. The results presented in Figure 3(a) immediately

highlight the impact of confinement, with both water uptake and λ being considerably smaller than that in bulk membranes (λ $20-15$ for various EWs at 98% RH).[16, 20] All three ionomers exhibit a characteristic nonlinear increase in both water uptake and λ with RH.[16] The 3M ionomers (825 EW and 1000 EW) have similar water uptake up to 70 % RH, suggesting similar anionic-group solvation profile and local ionomer morphology. At higher RH, 825 EW water uptake increases due to higher uptake of free-water molecules on account of high sulfonic-group density. Additionally, the fewer number of repeating TFE units between adjacent side chains in 825 EW results in a low backbone mechanical force opposing the swelling.[52-53] These differences at high RH due to sulfonic-group density are normalized when plotting λ versus RH where the 825 EW and 1000 EW curves coincide (Figure 3(b)). Nafion, however, has lower membrane water uptake and λ over the entire RH range, suggesting lower uptake of both bound and free water, which is potentially due to differences in morphology induced by side-chain chemistry.

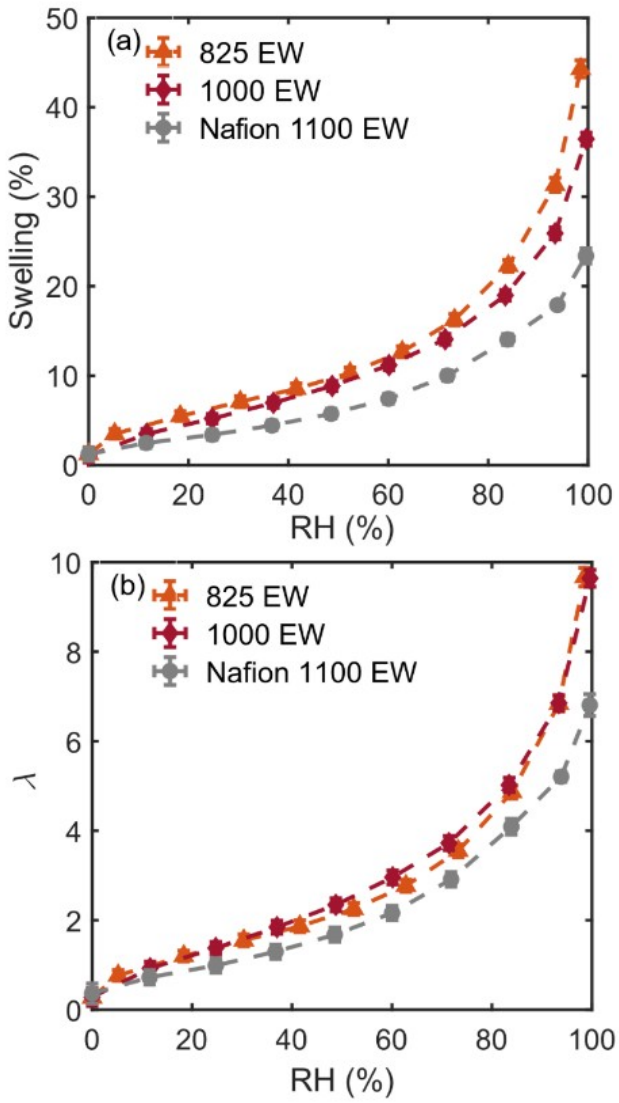

Figure 3: (a) Swelling ratio defined as a ratio of change in thin-film thickness (Δt¿ to initial thin-film thickness measured at 0 % RH ($\hat{\delta}_o$), and (b) Water content (λ¿ defined as moles of water uptake per mol SO^-_3 group versus RH. Measurements were performed on 20-nm films spin cast on Pt substrate at ambient temperature. Swelling ratio signifies the total water uptake by ionomer thin film, whereas λ is water uptake normalized to hydrophilic SO^-_3 groups.

The above *ex-situ* model-system trends compare nicely with the *in-situ* results presented in Figure 1. The high permeability of 825 EW, seen in the inverse slope of Figure 1, is consistent with the above swelling results, where higher water uptake has been correlated to increased dissolved-gas permeability.[16] However, it is interesting to note the large increase in slope *i.e.*, decrease in permeability from 825 EW to 1000 EW, despite similar λ and only a small difference in water uptake, compared to 1000 EW and Nafion that demonstrate similar permeabilities even with large differences in λ and water uptake. To explain this, we refer to polymer crystallinity, which also impacts dissolved-gas permeability.[16]

Ionomer crystallinity trends from GIWAXS characterization: Crystallinity, which increases with increasing TFE units between adjacent side-chains (high crystallinity in high EW ionomer), is known to impact dissolved-gas permeability negatively.[16, 22, 54] Increasing the number of TFE units also reduces the size and connectivity of hydrophilic anionic clusters, as measured by grazing incidence x-ray studies, thus restricting the dissolved-gas pathways and reducing permeability.[22] **Figure 4** (a) plots line-cuts from 2D GIWAXS patterns for Nafion and 825 EW ionomer thin films (reproduced from Kusoglu *et al.*[22]). Both ionomer chemistries exhibit crystallinity peak at high ionomer-film thickness (50 nm). However, on reducing the film thickness to 25 nm, only the Nafion film displays a clear crystalline peak, whereas no such feature exists for 825 EW. Thus, low water uptake, coupled with high ionomer crystallinity, and reduced size and connectivity of the hydrophilic anionic clusters, result in a significantly reduced dissolved-gas permeability of high EW ionomers (1000 EW and Nafion).

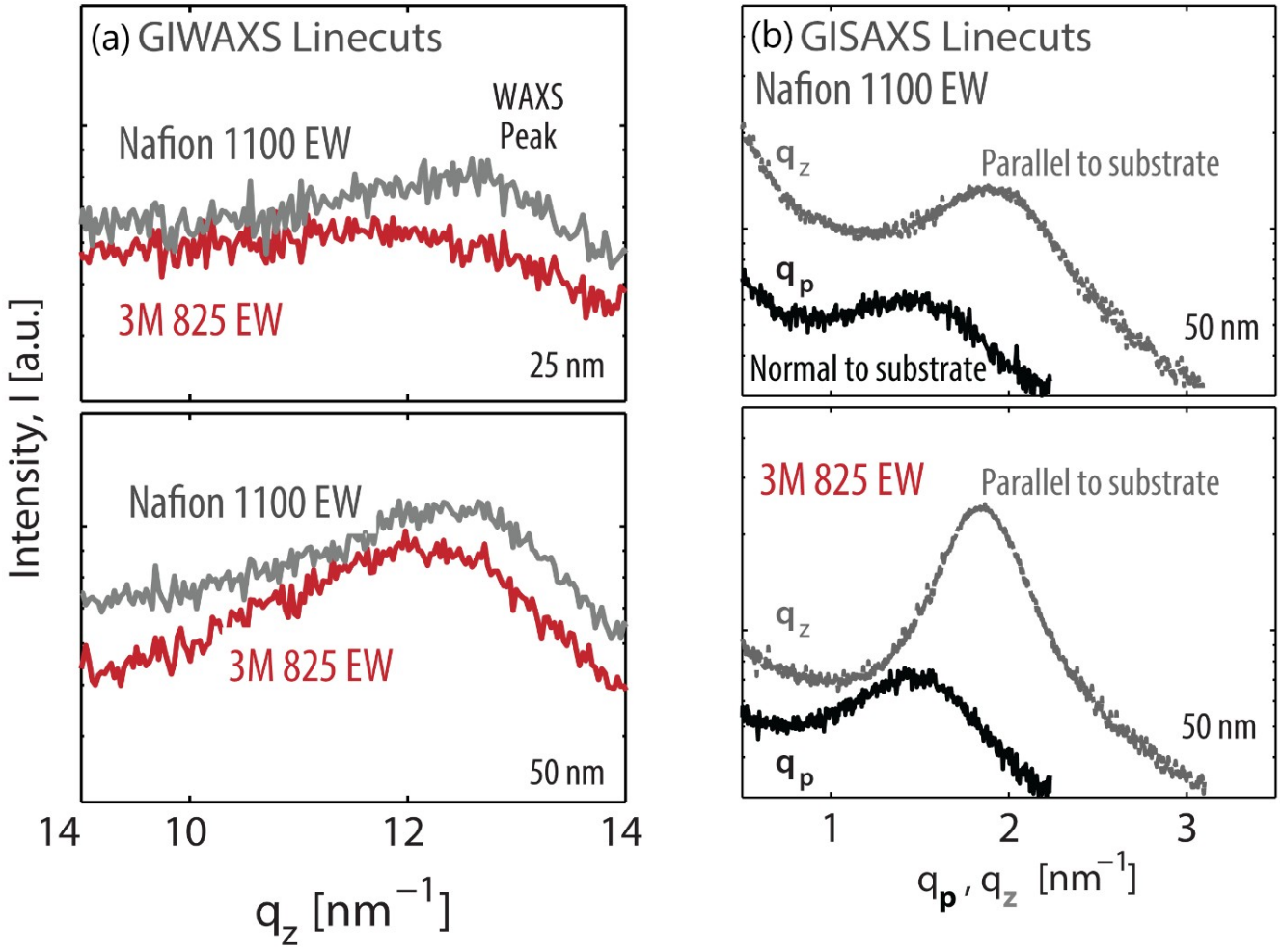

Figure 4: (a) Line cuts from 2D GIWAXS patterns in thickness direction at ambient temperature and RH (~35%). 25 nm Nafion (presented in grey) exhibits a clear crystallinity peak, while no such feature exists for lower EW ionomer (825 EW in red). (b) Line cuts (in both thickness and in-plane directions) from 2D GISAXS at ambient temperature and 100 % RH. The difference in peaks between the thickness and in-plane line cuts highlights anisotropy. Film thicknesses are listed. Reprinted in part with permission from reference 22. Copyright 2016, John Wiley and Sons"

Ionomer anisotropy trends from GISAXS characterization: Using GISAXS, Kusoglu *et al.*[22] examined domain spacing anisotropy in the thickness and in-plane directions, which can subsequently impact ionomer/Pt interactions. Both ionomers (825 EW and Nafion) were reported to have smaller domain spacing in the thickness direction compared to in-plane direction (Figure 4 (b), domain spacing is inversely proportional to the q-vector), with anisotropy increasing in thinner films. This result provides evidence for presence of confinement effects and stronger packing of chain/domains parallel to the substrate, which in turn can influence ionomer/substrate interactions and $R_{Pt/I}$.

Here we investigate anisotropy in domain spacing or preferential chain alignment by studying intensity (I) of GISAXS scattering patterns as a function of azimuthal angle χ. Higher intensity at low χ values (close to 0^o) represents preferential domain alignment in the thickness direction parallel to the substrate, whereas higher intensity at high χ values (close to 90^o) represents domain alignment perpendicular to the substrate.[23] Conversely, a uniform intensity represents an amorphous structure with random-chain alignment. **Figure 5** plots GISAXS scattering-pattern intensity as a function of χ for ionomer thin films cast on a Si substrate. Both 3M 825 EW and Nafion exhibit higher intensities at low $\chi's$, confirming preferential ionomer chain alignment parallel to the substrate. Most importantly, 3M 825 has higher intensity in the low χ-range compared to Nafion. This result demonstrates a higher degree of anisotropy in 3M 825. To quantify the degree of anisotropy, we calculate domain orientation parameter (OP),[23]

$$OP = \frac{\int I(\chi)\sin(\chi)\cos^2(\chi)\,d\chi}{\int I(\chi)\sin(\chi)\,d\chi} \tag{6}$$

For the χ range studied in this analysis, an isotropic film results in an OP equal to 0.509. The calculated OP for Nafion is 0.633 ± 0.058 and for 3M 825 is 0.664 ± 0.058, corresponding to a higher degree of anisotropy and chain alignment parallel to the substrate in 3M 825 EW. In a local environment with chain alignment parallel to the substrate, the ionomer anionic groups are expected to interact more strongly with the catalyst surface, resulting in higher $R_{Pt/I}$. These findings are in agreement with the findings from Ramaswamy *et al.*, where ionomer films with shorter side-chains exhibit smaller domain-spacing in the thickness direction, indicating tighter packing of chains/domains, and hence enabling more ionomer/Pt interactions.[41]

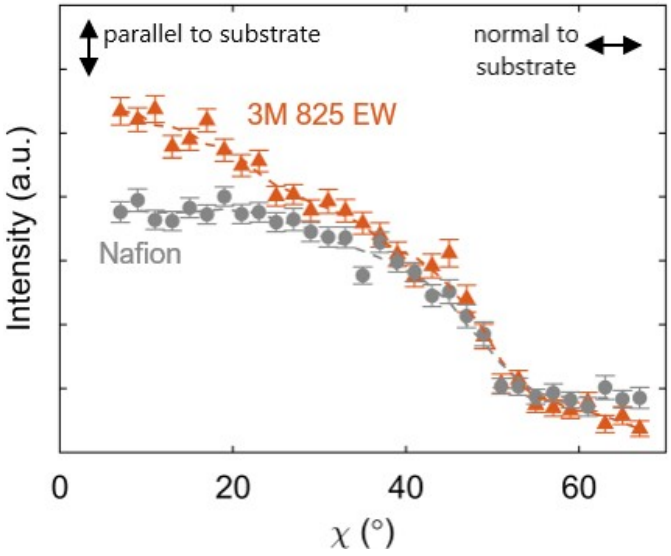

Figure 5: Integrated intensity (I) as a function of azimuthal angle, χ, for the GISAXS scattering patterns for 50 nm Nafion and 3M 825 EW cast on Si substrate and humidified at 100 % RH (GISAXS scattering pattern data reported in Figure 4). Error bars are generated from the 95 % confidence intervals of the peak fitting.

The above x-ray scattering experiments were performed on a Si substrate (potentially with an oxidized surface) with film thickness higher than those expected in PEFC electrodes. Although prior studies have demonstrated a significant impact of film thickness and substrate on ionomer properties and morphology,[16, 22] we expect the trends presented in Figures 4 and 5 to hold at least qualitatively in low film thicknesses relevant to PEFC electrodes. Additionally, oxidized Si substrate is a good indicator of the Pt/C catalyst particle surface where the carbon surface significantly dominates over the Pt surface, especially with low primary particle Pt loadings (as were utilized in the current study). In summary, we attribute the higher degree of anisotropy in 3M PFSA ionomers to the presence of shorter side chains as well as to higher density of sulfonic groups. This enables greater ionomer/substrate interactions, i.e., higher $R_{Pt/I}$, which is in-line with the limiting-current measurements in electrodes. These trends also agree with neutron reflectometry of Nafion on Pt and other x-ray studies on hydrophilic substrates.[23-24]

Overall, the *ex-situ* experiments accomplished with model ionomer thin films are consistent with the *in-situ* electrode results. Although the differences in specific system properties, such as film thickness and substrate, prevent direct 1:1 correlation between the two sets of experiments, the general agreement in trends lends credence for the *ex-situ* model systems to interrogate complex heterogeneous ones.

Ink effects at high I:C ratios

As highlighted in Figure 1, a strong nonlinear increase in R_{WE} is observed at higher I:C ratios, with the deviation from linear trend beginning at different I:C ratios for the three different ionomers (shown in **Figure 6)**. A possible explanation is that the electrode structure changes at

high I:C ratios, leading to a nonlinear increase in ionomer thin-film thickness with an increase in I:C ratio. PEFC electrodes are fabricated from complex colloidal ink dispersions consisting of ionomer, solvent (*e.g.*, water/nPA mixture as used in this study), and carbon-supported catalyst nanoparticles. Within inks, electrostatic and non-electrostatic specific interactions between ionomer/solvent, ionomer/particle, and solvent/particle govern aggregation behavior and ionomer morphology, which in turn control electrode structure.[42, 55-56]

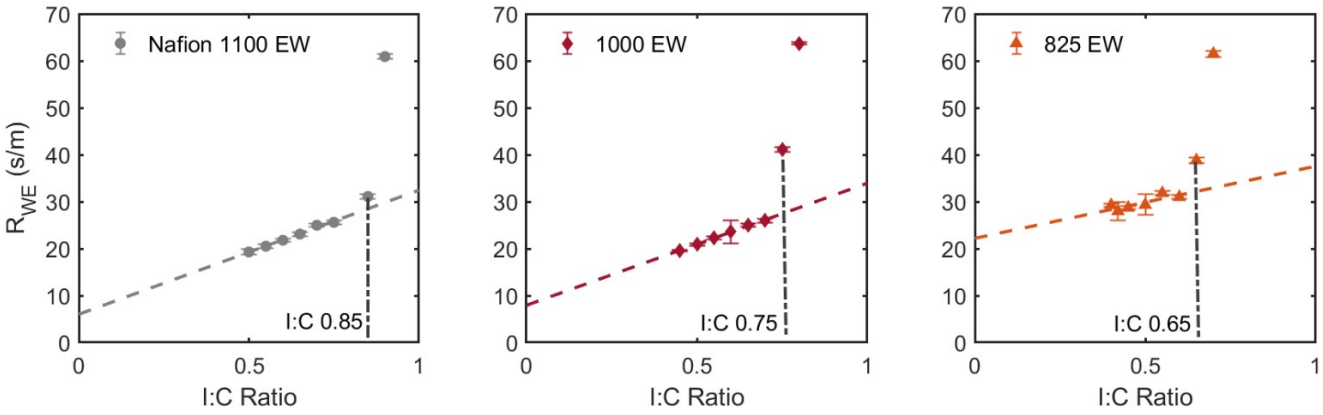

Figure 6: Non-linear increase in R_{WE} at higher I:C ratios. The non-linear increase begins at I:C ratio of 0.85 for Nafion, I:C ratio of 0.75 for 1000EW ionomer and 0.65 I:C ratio for 825 EW.

In this study, all parameters except ionomer content are maintained constant, suggesting that electrode structural changes can be attributed to the ionomer. However, the deviation from the linear trend of R_{WE} in Figure 6 starts at different I:C ratio for the three ionomers, demonstrating that the observed nonlinear behavior is not solely a function of ionomer mass content. To explain this, we examine ink pH and agglomerate size following the work of Berlinger *et al.*[42, 46, 55] Replotting the R_{WE} data as a function of sulfonate-anion concentration per gram carbon collapses

the curves in Figure 6 such that their nonlinear rises coincide at sulfonate-anion loading of 0.75 mmol/g_{carbon} (see **Figure 7**), which confirms the role of sulfonate-anion or proton-species interactions.

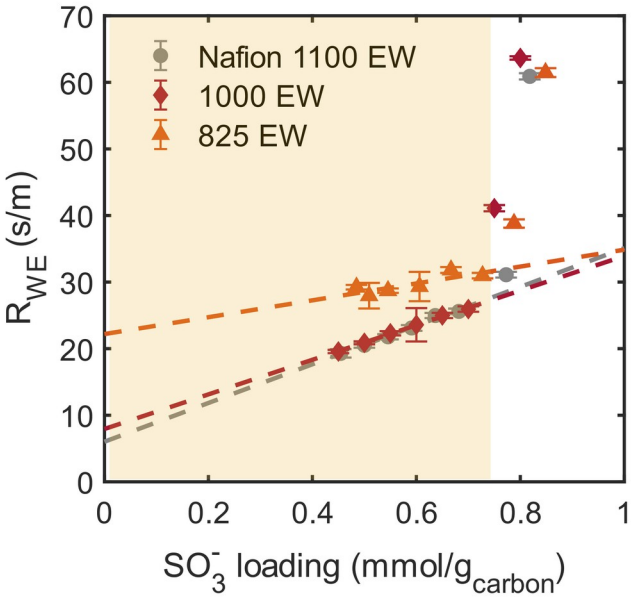

Figure 7: R_{WE} as a function of SO^-_3 loading per unit carbon weight. With increasing I:C ratio, sulfonate anion loading per unit carbon weight increases linearly. The region of linear increase (highlighted in yellow) coincides for the different ionomer chemistries.

To study the nature of ionomer interactions and the structural changes, zeta-potential measurements were performed to characterize the inks using Nafion as the test ionomer. Zeta potential is an indicator of colloidal stability: low magnitude zeta potentials can indicate small electrostatic repulsion between carbon agglomerates that result in greater agglomeration and vice versa. The ionomer in ink dispersions influence both electrostatic and non-electrostatic specific interactions, with the former stemming from the inherent acidity of the ionomer (*i.e.*, like an

inorganic acid), and the latter stemming from the specific hydrophobic/hydrophilic interactions with the catalyst particles, particularly through hydrophobic interactions with the graphitic Vulcan carbon support.[57]

We investigate specific ionomer/solvent and ionomer/catalyst interactions by studying inks with varying carbon to solvent weight ratio and catalyst primary particle Pt loading, respectively. As ionomer weight is normalized to the carbon weight in terms of I:C ratio, varying carbon to solvent weight ratio in inks also changes the ionomer to solvent weight ratio in a similar manner, thus probing specific ionomer/solvent interactions. Likewise, changing the catalyst-primary-particle loadings provides insight into specific ionomer/catalyst interactions. Zeta potential results are presented in **Figure 8**. For ink samples with 10 wt. % Pt/C and 0.025 wt. % carbon to solvent-weight ratios (corresponding to the electrode samples in Figure 6), a decrease in zeta potential magnitude from I:C ratio of 0.8 to 0.9 is observed, which coincides with the nonlinear increase in R_{WE}. Upon increasing the carbon to solvent weight ratio to 0.050 %, a similar trend persists (see Figure 8b), where the zeta potential magnitude decreases at I:C ratio of 0.9. This suggests that the observed changes are not caused by ionomer/solvent interactions. Conversely, varying the Pt/C ratio to 30 wt. % results in the decrease in zeta-potential magnitude to shift to a lower I:C ratio of 0.8 (Figure 8c).

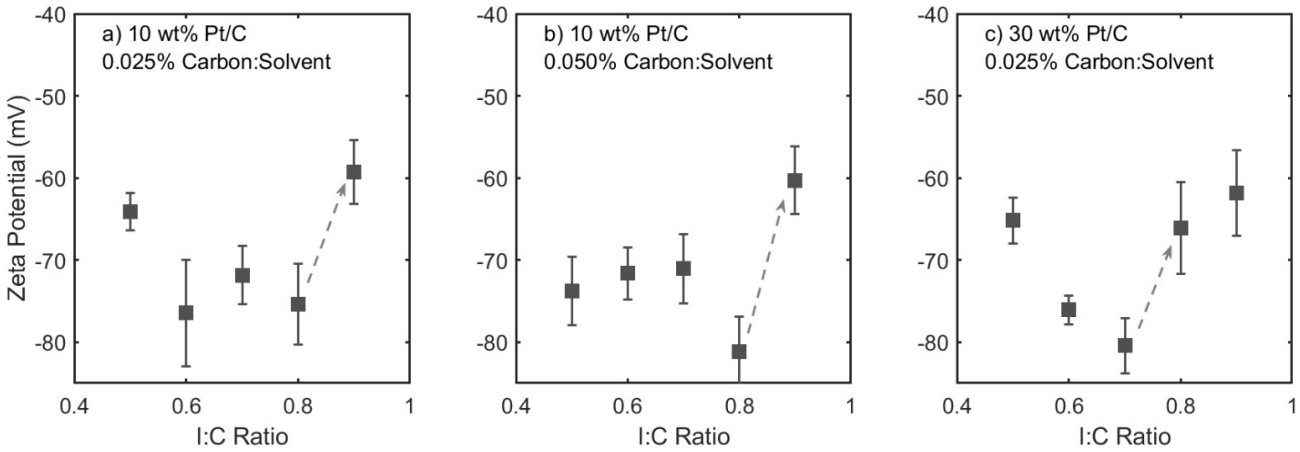

Figure 8: Zeta-potential measurements as a function of I:C ratio. (a) 10 wt. % Pt/C catalyst in 0.025 wt. % carbon: solvent weight ratio dispersion – base case ink, (b) concentrated ink with 10 wt. % Pt/C catalyst in 0.050 wt. % carbon: solvent weight ratio dispersion, and (c) 30 wt. % Pt/C catalyst (different catalyst) in 0.025 wt. % carbon: solvent weight ratio dispersion. Both inks with 10 wt. % Pt/C catalyst show a decrease in zeta-potential magnitude beyond I:C ratio of 0.8, whereas ink with 30 wt. % Pt/C ink exhibits this decrease at I:C ratio beyond 0.7.

R_{WE} of electrodes corresponding to ink dispersions with 10 and 30 wt. % Pt/C ink dispersions (Figure 8a and 8c) are shown in **Figure 9**. Once again, the change from linear to nonlinear trend in R_{WE} coincides with the changes in zeta-potential trend (note that R_{WE} values reported in Figure 1 for 10 wt. % Pt/C electrodes are slightly different from those reported in Figure 9 due to use of different ionomer stock dispersions – Nafion D521 and D2021, respectively). Thus, the ink ionomer/catalyst interactions induce electrode structural changes and resultant limiting-current behavior. As the carbon surface area decreases at higher Pt wt.%, the point of deviation from the linear trend shifts to lower I:C ratio. This observation suggests that specific carbon/ionomer

hydrophobic interactions might be responsible. Note that low I:C ratio inks also have low zeta-potential magnitude, but align with the linear trend; this behavior is currently not understood. Exact correlations between zeta potential and electrode structure are beyond the scope of this study.

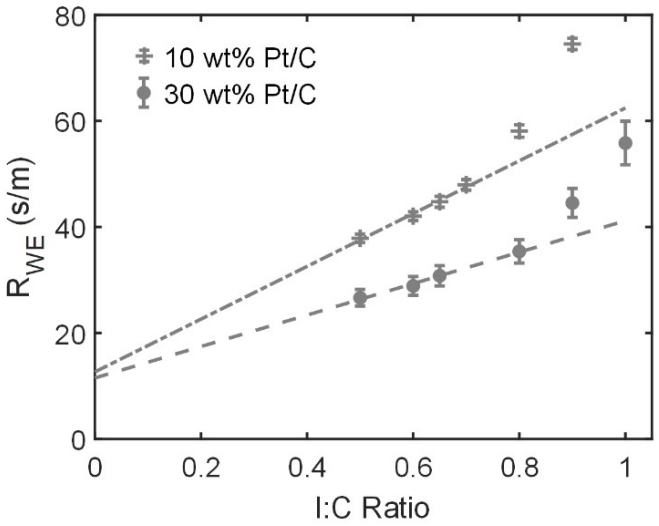

Figure 9: R_{WE} for samples fabricated from 10 wt. % Pt/C and 30 wt. % Pt/C in 0.025 wt. % carbon: solvent weight ratio dispersion. The nonlinear trend starts at I:C ratio of 0.9 for 10 wt. % Pt/C and 0.8 I:C ratio for 30 wt. % Pt/C, coinciding with jumps in zeta-potential measurements.

CONCLUSION

Reduction of local gas-transport resistance in PEFC electrodes is essential to improve high-current-density performance and achieve reasonable power output from low Pt-loaded electrodes, thus making them commercially viable. Ionomer thin films are the primary source of this local gas-transport resistance due to low ionomer thin-film permeability (compared to bulk ionomer) and interfacial resistance due to catalyst/sulfonate interactions. *In-situ* measurements of

anion adsorption on Pt and ionomer water uptake (in terms of ionomer conductivity) validate the above findings. Results from *ex-situ* model studies on ionomer thin-films, such as swelling and x-ray scattering correlate positively with the *in-situ* results, thereby affirming their applicability as powerful tools to study complex heterogenous systems like PEFC electrodes. Specific conclusions from this study are:

1. Electrode transport resistance increases with I:C ratio for all examined ionomers. Since electrode resistance is primarily contributed from local gas-transport resistance for low Pt-loaded electrodes with low electrode thickness, we attribute this behavior to formation of thicker ionomer thin films at higher ionomer contents thus resulting in higher dissolved-gas diffusion-resistance. This finding also suggests that lowering the I:C ratio while maintaining triple-percolated pathways needed for catalyst utilization is a viable means for improving PEFC performance.
2. Ionomer chemistry, particularly EW, can influence the component and overall local gas-transport resistance. Low-EW ionomers with high ion-exchange capacity and high side-chain density have low crystallinity and promote greater water uptake that enhance thin-film permeability. However, low EW ionomers also cause greater ionomer-Pt interactions and hence higher interfacial resistance. Additionally, side-chain length impacts local morphological behavior, with shorter sidechains providing better chain alignment and sulfonic-group/substrate interactions; thus, increasing interfacial resistance. These suggest that developing ionomers with bulky groups and large free volume to enhance transport and impede the interactions of side chains with the catalyst surface is a possible means for improving PEFC performance.[58-60]

3. Ionomer content influences electrode morphology that in turn, impacts electrode gas-transport resistance. Above a threshold sulfonic-group density normalized to carbon content of 0.75 mmol/g_{carbon}, a sudden nonlinear increase occurs in the electrode gas-transport resistance. Corresponding inks also demonstrate a sudden decrease in zeta-potential magnitude at this critical ratio. This threshold limit potentially indicates the tipping point at which the dominant interactions in inks change. Tuning ink parameters may enable electrode fabrication with optimum reactant transport pathways.

ASSOCIATED CONTENT

Supporting Information: WE roughness factor (r_f) measurements, linear regression data (slopes and intercept magnitudes) of R_{WE} vs I:C ratio plots, corresponding to figure 1, WE gas-transport model, experimental details, and limiting-current measurement data.

AUTHOR INFORMATION

Corresponding Author

*Adam Z. Weber: azweber@lbl.gov

Present Addresses

Energy Conversion Group, Lawrence Berkeley National Laboratory, Berkeley, CA 94720

ACKNOWLEDGMENT

We would like to thank Sarah Berlinger for helpful discussions and insights, and Mike Yandrasits and Andrew Haug at 3M Company for provided ionomer dispersions. The work was supported by the Fuel Cell Performance and Durability Consortium (FC-PAD) and subsequently the Million Mile Fuel Cell Truck (M2FCT) Consortium, by the Hydrogen and Fuel Cell

Technologies Office (HFTO), and by the Office of Energy Efficiency and Renewable Energy (EERE), of the U.S. Department of Energy under contract number DE-AC02-05CH11231. We thank Mr. Yongzhen Qi for collecting ionic-conductivity data. Prof. Zenyuk acknowledges support from the Department of Energy, Office of Energy Efficiency and Renewable Energy (EERE), Award Number DE-EE0007270.

REFERENCES

(1) Ryan, E. M.; Mukherjee, P. P. Mesoscale Modeling in Electrochemical Devices—a Critical Perspective. *Progress in Energy and Combustion Science* **2019,** *71*, 118-142.
(2) Sun, H.; Zhu, J.; Baumann, D.; Peng, L.; Xu, Y.; Shakir, I.; Huang, Y.; Duan, X. Hierarchical 3d Electrodes for Electrochemical Energy Storage. *Nature Reviews Materials* **2019,** *4* (1), 45-60.
(3) Berlinger, S. A.; Garg, S.; Weber, A. Z. Multicomponent, Multiphase Interactions in Fuel Cell Inks. *Current Opinion in Electrochemistry* **2021**, 100744.
(4) Xie, J.; Wood, D. L.; More, K. L.; Atanassov, P.; Borup, R. L. Microstructural Changes of Membrane Electrode Assemblies During Pefc Durability Testing at High Humidity Conditions. *J Electrochem Soc* **2005,** *152* (5), A1011-A1020.
(5) More, K.; Borup, R.; Reeves, K. Identifying Contributing Degradation Phenomena in Pem Fuel Cell Membrane Electride Assemblies Via Electron Microscopy. *ECS Trans* **2006,** *3* (1), 717-733.
(6) Berejnov, V.; Susac, D.; Stumper, J.; Hitchcock, A. P. 3d Chemical Mapping of Pem Fuel Cell Cathodes by Scanning Transmission Soft X-Ray Spectrotomography. *ECS Trans* **2013,** *50* (2), 361-368.
(7) Greszler, T. A.; Caulk, D.; Sinha, P. The Impact of Platinum Loading on Oxygen Transport Resistance. *J Electrochem Soc* **2012,** *159* (12), F831-F840, DOI: 10.1149/2.061212jes.
(8) Lopez-Haro, M.; Guetaz, L.; Printemps, T.; Morin, A.; Escribano, S.; Jouneau, P. H.; Bayle-Guillemaud, P.; Chandezon, F.; Gebel, G. Three-Dimensional Analysis of Nafion Layers in Fuel Cell Electrodes. *Nat Commun* **2014,** *5*, 5229, DOI: 10.1038/ncomms6229.
(9) Cetinbas, F. C.; Ahluwalia, R. K.; Kariuki, N. N.; Myers, D. J. Agglomerates in Polymer Electrolyte Fuel Cell Electrodes: Part I. Structural Characterization. *J Electrochem Soc* **2018,** *165* (13), F1051-F1058.
(10) Cetinbas, F. C.; Ahluwalia, R. K.; Kariuki, N.; De Andrade, V.; Fongalland, D.; Smith, L.; Sharman, J.; Ferreira, P.; Rasouli, S.; Myers, D. J. Hybrid Approach Combining Multiple Characterization Techniques and Simulations for Microstructural Analysis of Proton Exchange Membrane Fuel Cell Electrodes. *J Power Sources* **2017,** *344*, 62-73, DOI: 10.1016/j.jpowsour.2017.01.104.
(11) Cetinbas, F. C.; Wang, X.; Ahluwalia, R. K.; Kariuki, N. N.; Winarski, R. P.; Yang, Z.; Sharman, J.; Myers, D. J. Microstructural Analysis and Transport Resistances of Low-Platinum-Loaded Pefc Electrodes. *J Electrochem Soc* **2017,** *164* (14), F1596-F1607.
(12) Weber, A. Z.; Kusoglu, A. Unexplained Transport Resistances for Low-Loaded Fuel-Cell Catalyst Layers. *J Mater Chem A* **2014,** *2* (41), 17207-17211, DOI: 10.1039/c4ta02952f.
(13) Kongkanand, A.; Mathias, M. F. The Priority and Challenge of High-Power Performance of Low-Platinum Proton-Exchange Membrane Fuel Cells. *J Phys Chem Lett* **2016,** *7* (7), 1127-1137, DOI: 10.1021/acs.jpclett.6b00216.
(14) Nonoyama, N.; Okazaki, S.; Weber, A. Z.; Ikogi, Y.; Yoshida, T. Analysis of Oxygen-Transport Diffusion Resistance in Proton-Exchange-Membrane Fuel Cells. *J Electrochem Soc* **2011,** *158* (4), B416-B423, DOI: Doi 10.1149/1.3546038.

(15) Sakai, K.; Sato, K.; Mashio, T.; Ohma, A.; Yamaguchi, K.; Shinohara, K. Analysis of Reactant Gas Transport in Catalyst Layers; Effect of Pt-Loadings. *ECS Trans* **2009,** *25* (1), 1193-1201.
(16) Kusoglu, A.; Weber, A. Z. New Insights into Perfluorinated Sulfonic-Acid Lonomers. *Chem. Rev.* **2017,** *117* (3), 987-1104, DOI: 10.1021/acs.chemrev.6b00159.
(17) Ono, Y.; Ohma, A.; Shinohara, K.; Fushinobu, K. Influence of Equivalent Weight of Ionomer on Local Oxygen Transport Resistance in Cathode Catalyst Layers. *J Electrochem Soc* **2013,** *160* (8), F779-F787, DOI: 10.1149/2.040308jes.
(18) Eastman, S. A.; Kim, S.; Page, K. A.; Rowe, B. W.; Kang, S.; Soles, C. L.; Yager, K. G. Effect of Confinement on Structure, Water Solubility, and Water Transport in Nafion Thin Films. *Macromolecules* **2012,** *45* (19), 7920-7930.
(19) Dishari, S. K.; Hickner, M. A. Antiplasticization and Water Uptake of Nafion Thin Films. *ACS Macro Letters* **2012,** *1* (2), 291-295.
(20) Kusoglu, A.; Kushner, D.; Paul, D. K.; Karan, K.; Hickner, M. A.; Weber, A. Z. Impact of Substrate and Processing on Confinement of Nafion Thin Films. *Adv Funct Mater* **2014,** *24* (30), 4763-4774.
(21) Modestino, M. A.; Paul, D. K.; Dishari, S.; Petrina, S. A.; Allen, F. I.; Hickner, M. A.; Karan, K.; Segalman, R. A.; Weber, A. Z. Self-Assembly and Transport Limitations in Confined Nafion Films. *Macromolecules* **2013,** *46* (3), 867-873, DOI: 10.1021/ma301999a.
(22) Kusoglu, A.; Dursch, T. J.; Weber, A. Z. Nanostructure/Swelling Relationships of Bulk and Thin-Film Pfsa Ionomers. *Adv Funct Mater* **2016,** *26* (27), 4961-4975, DOI: 10.1002/adfm.201600861.
(23) Tesfaye, M.; Kushner, D. I.; Kusoglu, A. Interplay between Swelling Kinetics and Nanostructure in Perfluorosulfonic Acid Thin-Films: Role of Hygrothermal Aging. *ACS Applied Polymer Materials* **2019,** *1* (4), 631-635.
(24) Kushner, D. I.; Kusoglu, A.; Podraza, N. J.; Hickner, M. A. Substrate-Dependent Molecular and Nanostructural Orientation of Nafion Thin Films. *Adv Funct Mater* **2019,** *29* (37), 1902699.
(25) Kongkanand, A. Interfacial Water Transport Measurements in Nafion Thin Films Using a Quartz-Crystal Microbalance. *The Journal of Physical Chemistry C* **2011,** *115* (22), 11318-11325.
(26) Siroma, Z.; Kakitsubo, R.; Fujiwara, N.; Ioroi, T.; Yamazaki, S.-i.; Yasuda, K. Depression of Proton Conductivity in Recast Nafion® Film Measured on Flat Substrate. *J Power Sources* **2009,** *189* (2), 994-998.
(27) Paul, D. K.; McCreery, R.; Karan, K. Proton Transport Property in Supported Nafion Nanothin Films by Electrochemical Impedance Spectroscopy. *J Electrochem Soc* **2014,** *161* (14), F1395-F1402.
(28) Kudo, K.; Morimoto, Y. Analysis of Oxygen Transport Resistance of Nafion Thin Film on Pt Electrode. *ECS Transactions* **2013,** *50* (2), 1487-1494.
(29) Subbaraman, R.; Strmcnik, D.; Paulikas, A. P.; Stamenkovic, V. R.; Markovic, N. M. Oxygen Reduction Reaction at Three-Phase Interfaces. *Chemphyschem* **2010,** *11* (13), 2825-2833, DOI: 10.1002/cphc.201000190.
(30) Shinozaki, K.; Zack, J. W.; Pylypenko, S.; Richards, R. M.; Pivovar, B. S.; Kocha, S. S. Benchmarking the Oxygen Reduction Reaction Activity of Pt-Based Catalysts Using Standardized Rotating Disk Electrode Methods. *Int J Hydrogen Energ* **2015,** *40* (46), 16820-16830, DOI: 10.1016/j.ijhydene.2015.08.024.
(31) Kodama, K.; Shinohara, A.; Hasegawa, N.; Shinozaki, K.; Jinnouchi, R.; Suzuki, T.; Hatanaka, T.; Morimoto, Y. Catalyst Poisoning Property of Sulfonimide Acid

Ionomer on Pt (111) Surface. *J Electrochem Soc* **2014,** *161* (5), F649-F652, DOI: 10.1149/2.051405jes.
(32) Jinnouchi, R.; Kudo, K.; Kitano, N.; Morimoto, Y. Molecular Dynamics Simulations on O-2 Permeation through Nafion Lonomer on Platinum Surface. *Electrochim Acta* **2016,** *188*, 767-776, DOI: 10.1016/j.electacta.2015.12.031.
(33) Iden, H.; Takaichi, S.; Furuya, Y.; Mashio, T.; Ono, Y.; Ohma, A. Relationship between Gas Transport Resistance in the Catalyst Layer and Effective Surface Area of the Catalyst. *J Electroanal Chem* **2013,** *694*, 37-44.
(34) Garrick, T. R.; Moylan, T. E.; Yarlagadda, V.; Kongkanand, A. Characterizing Electrolyte and Platinum Interface in Pem Fuel Cells Using Co Displacement. *J Electrochem Soc* **2017,** *164* (2), F60-F64, DOI: 10.1149/2.0551702jes.
(35) Schuler, T.; Chowdhury, A.; Freiberg, A. T. S.; Sneed, B. T.; Spingler, F. B.; Tucker, M. C.; More, K.; Radke, C. J.; Weber, A. Z. Fuel-Cell Catalyst-Layer Resistance Via Hydrogen Limiting-Current Measurements. *J Electrochem Soc* **2019,** *166* (7), F3020-F3031, DOI: 10.1149/2.0031907jes.
(36) Chowdhury, A.; Radke, C. J.; Weber, A. Z. Transport Resistances in Fuel-Cell Catalyst Layers. *ECS Trans* **2017,** *80* (8), 321-333.
(37) Chowdhury, A.; Darling, R. M.; Radke, C. J.; Weber, A. Z. Modeling Water Uptake and Pt Utilization in High Surface Area Carbon. *ECS Trans* **2019,** *92* (8), 247-259.
(38) Katzenberg, A.; Chowdhury, A.; Fang, M.; Weber, A. Z.; Okamoto, Y.; Kusoglu, A.; Modestino, M. A. Highly Permeable Perfluorinated Sulfonic Acid Ionomers for Improved Electrochemical Devices: Insights into Structure–Property Relationships. *Journal of the American Chemical Society* **2020,** *142* (8), 3742-3752.
(39) Schaberg, M. S.; Abulu, J. E.; Haugen, G. M.; Emery, M. A.; O'Conner, S. J.; Xiong, P. N.; Hamrock, S. New Multi Acid Side-Chain Ionomers for Proton Exchange Membrane Fuel Cells. *ECS Trans* **2010,** *33* (1), 627-633.
(40) Yandrasits, M.; Lindell, M.; Peppin, D.; Komlev, A.; Hamrock, S.; Haugen, G.; Fort, E.; Kalstabakken, K. Chemical Stability of Perfluorobis (Sulfonyl) Imide-Acid (Pfia) Ionomers in Open Circuit Voltage (Ocv) Accelerated Test Conditions. *J Electrochem Soc* **2018,** *165* (6), F3261-F3270.
(41) Ramaswamy, N.; Kumaraguru, S.; Koestner, R.; Fuller, T.; Gu, W.; Kariuki, N.; Myers, D.; Dudenas, P. J.; Kusoglu, A. Editors' Choice—Ionomer Side Chain Length and Equivalent Weight Impact on High Current Density Transport Resistances in Pemfc Cathodes. *J Electrochem Soc* **2021,** *168* (2), 024518.
(42) Berlinger, S. A.; McCloskey, B. D.; Weber, A. Z. Inherent Acidity of Perfluorosulfonic Acid Ionomer Dispersions and Implications for Ink Aggregation. *The Journal of Physical Chemistry B* **2018,** *122* (31), 7790-7796.
(43) Spingler, F. B.; Phillips, A.; Schuler, T.; Tucker, M. C.; Weber, A. Z. Investigating Fuel-Cell Transport Limitations Using Hydrogen Limiting Current. *Int J Hydrogen Energ* **2017,** *42* (19), 13960-13969, DOI: 10.1016/j.ijhydene.2017.01.036.
(44) Sabarirajan, D. C.; Liu, J.; Qi, Y.; Perego, A.; Haug, A. T.; Zenyuk, I. V. Determining Proton Transport in Pseudo Catalyst Layers Using Hydrogen Pump Dc and Ac Techniques. *J Electrochem Soc* **2020,** *167* (8), 084521.
(45) Tesfaye, M.; MacDonald, A. N.; Dudenas, P. J.; Kusoglu, A.; Weber, A. Z. Exploring Substrate/Ionomer Interaction under Oxidizing and Reducing Environments. *Electrochemistry Communications* **2018,** *87*, 86-90.
(46) Berlinger, S. A.; Dudenas, P. J.; Bird, A.; Chen, X.; Freychet, G.; McCloskey, B. D.; Kusoglu, A.; Weber, A. Z. Impact of Dispersion Solvent on Ionomer Thin Films and Membranes. *ACS Applied Polymer Materials* **2020,** *2* (12), 5824-5834.

(47) Gebel, G.; Lambard, J. Small-Angle Scattering Study of Water-Swollen Perfluorinated Ionomer Membranes. *Macromolecules* **1997,** *30* (25), 7914-7920.
(48) Yoneda, Y. Anomalous Surface Reflection of X Rays. *Physical review* **1963,** *131* (5), 2010.
(49) Padgett, E.; Andrejevic, N.; Liu, Z.; Kongkanand, A.; Gu, W.; Moriyama, K.; Jiang, Y.; Kumaraguru, S.; Moylan, T.; Kukreja, R.; Muller, D. Connecting Fuel Cell Catalyst Nanostructure and Accessibility Using Quantitative Cryo-Stem Tomography. *J Electrochem Soc* **2018,** *165* (3), F173-F180, DOI: 10.1149/2.0541803jes.
(50) Chen, Q.-S.; Solla-Gullón, J.; Sun, S.-G.; Feliu, J. M. The Potential of Zero Total Charge of Pt Nanoparticles and Polycrystalline Electrodes with Different Surface Structure: The Role of Anion Adsorption in Fundamental Electrocatalysis. *Electrochim Acta* **2010,** *55* (27), 7982-7994.
(51) Huang, J.; Malek, A.; Zhang, J.; Eikerling, M. H. Non-Monotonic Surface Charging Behavior of Platinum: A Paradigm Change. *The Journal of Physical Chemistry C* **2016,** *120* (25), 13587-13595.
(52) Kusoglu, A.; Savagatrup, S.; Clark, K. T.; Weber, A. Z. Role of Mechanical Factors in Controlling the Structure–Function Relationship of Pfsa Ionomers. *Macromolecules* **2012,** *45* (18), 7467-7476.
(53) Crothers, A. R.; Darling, R. M.; Kusoglu, A.; Radke, C. J.; Weber, A. Z. Theory of Multicomponent Phenomena in Cation-Exchange Membranes: Part I. Thermodynamic Model and Validation. *J Electrochem Soc* **2020,** *167* (1), 013547.
(54) Giffin, G. A.; Haugen, G. M.; Hamrock, S. J.; Di Noto, V. Interplay between Structure and Relaxations in Perfluorosulfonic Acid Proton Conducting Membranes. *J Am Chem Soc* **2013,** *135* (2), 822-834.
(55) Hatzell, K. B.; Dixit, M. B.; Berlinger, S. A.; Weber, A. Z. Understanding Inks for Porous-Electrode Formation. *J Mater Chem A* **2017,** *5* (39), 20527-20533.
(56) Van Cleve, T.; Khandavalli, S.; Chowdhury, A.; Medina, S.; Pylypenko, S.; Wang, M.; More, K. L.; Kariuki, N.; Myers, D. J.; Weber, A. Z. Dictating Pt-Based Electrocatalyst Performance in Polymer Electrolyte Fuel Cells, from Formulation to Application. *ACS applied materials & interfaces* **2019,** *11* (50), 46953-46964.
(57) Berlinger, S. A.; McCloskey, B. D.; Weber, A. Z. Probing Ionomer Interactions with Electrocatalyst Particles in Solution. *ACS Energy Letters* **2021,** *6*, 2275-2282.
(58) Peressin, N.; Adamski, M.; Holdcroft, S. Effect of Steric Constraints on the Physico-Electrochemical Properties of Sulfonated Polyaromatic Copolymers. *Polymer International* **2021,** *70* (1), 96-106.
(59) Farzin, S.; Sarella, A.; Yandrasits, M. A.; Dishari, S. K. Fluorocarbon-Based Ionomers with Single Acid and Multiacid Side Chains at Nanothin Interfaces. *The Journal of Physical Chemistry C* **2019,** *123* (51), 30871-30884.
(60) Shrivastava, U. N.; Fritzsche, H.; Karan, K. Interfacial and Bulk Water in Ultrathin Films of Nafion, 3m Pfsa, and 3m Pfia Ionomers on a Polycrystalline Platinum Surface. *Macromolecules* **2018,** *51* (23), 9839-9849.

FOR TABLE OF CONTENTS ONLY